



FRONTIERS ARTICLE

On the hydration and hydrolysis of carbon dioxide

Alice H. England^{a,b}, Andrew M. Duffin^{a,b}, Craig P. Schwartz^{a,b}, Janel S. Uejio^{a,b},
David Prendergast^{c,*}, Richard J. Saykally^{a,b,*}

^a Department of Chemistry, University of California, Berkeley, CA 94720, USA

^b Chemical Sciences Division, Lawrence Berkeley National Laboratory, Berkeley, CA 94720, USA

^c Molecular Foundry, Lawrence Berkeley National Laboratory, Berkeley, CA 94720, USA

ARTICLE INFO

Article history:

Available online 24 August 2011

ABSTRACT

The dissolution of carbon dioxide in water and the ensuing hydrolysis reactions are of profound importance for understanding the behavior and control of carbon in the terrestrial environment. The first X-ray absorption spectra of aqueous carbonate have been measured at three different pH values to characterize the evolution of electronic structure of carbonate, bicarbonate, carbonic acid and dissolved CO₂. The corresponding carbon K-edge core-level spectra were calculated using a first-principles electronic structure approach which samples molecular dynamics trajectories. Measured and calculated spectra are in excellent agreement. Each species exhibits similar, but distinct, spectral features which are interpreted in terms of the relative C–O bond strengths, molecular configuration, and hydration strength.

© 2011 Elsevier B.V. All rights reserved.

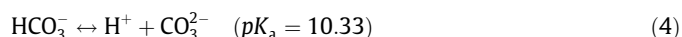
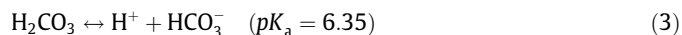
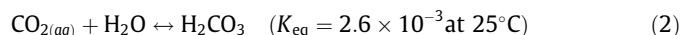
1. Introduction

The hydrolysis of carbon dioxide (CO₂) to form carbonic acid and the subsequent speciation to bicarbonate and carbonate is a fundamental process that has been studied extensively. From a geological perspective, carbonic acid is the most abundant terrestrial acid, while bicarbonate and carbonate are the primary contributors to total alkalinity in natural waters. These dissolved carbonate species participate in numerous reactions that have vital implications in rock weathering, mineral precipitation, ocean acidification and climate change. New technologies are emerging to mitigate global warming by exploiting methods for capture and storage of excess CO₂, such as the metal-organic-frameworks (MOFs) developed to selectively trap CO₂ gas [1] or pumping CO₂ into underground salt-water reservoirs [2].

Aqueous carbonate chemistry not only governs the terrestrial carbon cycle, but it also maintains the delicate pH balance required in mammalian biological systems. The carbonate/bicarbonate/CO₂ buffer system regulates blood pH, and is also responsible for CO₂ transport in the body and ion mobility across cell membranes. The importance of calcium carbonate in biomineralization processes has led to extensive study of its nucleation and precipitation dynamics in supersaturated solutions [3,4]. Seawater carbonate chemistry dictates the uptake of CO₂ in surface waters, and the consequent carbonate saturation plays a major role in the calcification of ocean organisms and ecosystems [5]. Furthermore, the

influence of the aqueous carbonate system extends to the astronomical realm. Upon irradiation, CO₂–H₂O deposits in outer space are converted to carbonic acid, which has also been identified as a possible species present on several planetary surfaces [6].

Understanding the molecular-scale details of carbonate, bicarbonate, carbonic acid, and CO₂ behavior in these various environments is critical to the development and success of future strategies aimed at maintaining or mitigating these natural carbon processes. The overall reactions [7] for carbon dioxide dissolution, hydrolysis, and equilibrium are:



There have been many studies addressing these species, with research on carbonate solubility dating back to as early as 1902 [8], and extensive characterization of this fundamental system continuing throughout the past century to document the relevant equilibria, kinetics, thermodynamics, and structural properties. Notable areas include Raman and IR experiments of carbonate species in solution [9–12], investigation into solubility and hydration mechanisms [13–15], and analysis of ion pairing [16–18]. More recently, theoretical studies of the aqueous carbonate system have worked to elucidate mechanistic details of the equilibrium reactions as well as hydration processes through molecular dynamics simulations and quantum calculations [14,19–23].

* Corresponding authors. Address: Department of Chemistry, University of California, Berkeley, CA 94720, USA. Fax: +1 510 642 8566 (R.J. Saykally).

E-mail addresses: dgprendergast@lbl.gov (D. Prendergast), saykally@berkeley.edu (R.J. Saykally)

The nature of carbonic acid itself has been of central interest. While its observation in the gas phase is well-documented, it was long debated whether it exists as a short-lived intermediate or only as a transition state that cannot be isolated. Earlier studies on the aqueous form were able to identify carbonic acid in ice matrices via FT-IR spectroscopy, either as a result of bicarbonate protonation at low temperatures, or irradiation of solid $\text{CO}_2\text{-H}_2\text{O}$ ices [6]. More recent studies succeeded in spectroscopic detection of carbonic acid in water, including Raman measurements [24] and ultrafast IR experiments [25]. Alternative detection methods with clear spectral signatures for carbonic acid are crucial to the future characterization of this short-lived species.

Near edge X-ray absorption fine structure spectroscopy (NEXAFS), is an atom-specific probe of not only the electronic structure of a molecule, but also of its local chemical environment, making it an ideal method for detailed characterization of hydration interactions. Previous NEXAFS studies were restricted to gaseous CO_2 [26], and carbonate adsorbed to a surface [27] or in various solid mineral forms [28], by the difficulties inherent in addressing liquid samples. Here we report the first measurement of the carbon K-edge NEXAFS spectra for aqueous carbonates, facilitated by the use of liquid microjet technology [29]. We combine molecular dynamics (MD) simulations with a first principles density functional theory (DFT) method to model and interpret the measured NEXAFS spectra [30,31], gaining new and detailed insights into the nature of aqueous carbonate species.

2. Materials and methods

2.1. Experimental

Sodium carbonate was obtained commercially from Sigma–Aldrich in the crystalline form of 99.0% purity. A 1 M solution was prepared with 18 M Ω /cm resistivity water, at an initial pH of 12. To access the lower pH regions, the carbonate samples were mixed with appropriate ratios of 1 M HCl in a dual syringe pump system (Teledyne–Isco) by adjusting the relative flow rates. Based on reactions (1)–(4) and associated equilibrium constants, the initial equilibrium composition as a function of pH was as follows: pH = 12 (98% carbonate and 2% bicarbonate); pH = 8.5 (98% bicarbonate and 2% carbonic acid/ CO_2); pH = 3 (100% carbonic acid/ CO_2). Because the relevant reaction rates are not known, it is not possible to reliably estimate the adjusted composition when the liquid microjet is injected into vacuum. Moreover, to actually measure these concentrations *in situ* would require a different experiment.

The NEXAFS experiments were conducted at Beamline 8.0.1. at the Advanced Light Source (Lawrence Berkeley National Labs, Berkeley, CA). A detailed description of the experiment has been published previously [29]. Briefly, in the main vacuum chamber a liquid microjet stream is produced by a 30 μm fused silica capillary tip pressurized with the syringe pump. Shortly after the sample leaves the jet tip, it is intersected with an intense, tunable X-ray beam over the carbon K-edge energy range (280–320 eV). The total electron yield (TEY) was collected with a 2.1 kV biased copper electrode as representative of the bulk liquid spectra. Similarly, the vapor phase spectra were obtained by positioning the jet slightly above or below the incident X-ray beam. In order to account for intensity fluctuations, the TEY signal was normalized to an I_0 collected from a gold mesh located further up the beamline. The background vapor signals were subtracted from the spectra, which were subsequently area-normalized for comparison.

2.2. Molecular dynamics simulations

AMBER 9 [32] was used to perform classical MD simulations for gaseous and dissolved CO_2 , and Quantum Mechanic/Molecular Mechanics (QM/MM) trajectories for carbonate, bicarbonate, and carbonic acid. Classical MD calculations employed the default ff99SB force field while the PM3 method was used for the semi-empirical QM/MM calculations. For all systems, ~ 90 TIP3P waters were added and the MD simulations were run in periodic boundary conditions for 10 ns. 100 uncorrelated snapshots were chosen from each trajectory to represent a sufficient sampling of molecular motions. Additionally, first principles molecular dynamics (FPMD), within the Born–Oppenheimer approximation, was performed on carbonate to verify the accuracy of the QM/MM simulation. We used the Quantum-ESPRESSO package [33], sampling the dynamics of the electronic ground state for 2.5 ps using the Perdew–Burke–Ernzerhof form of the generalized-gradient approximation (PBE GGA functional) [34].

2.3. First principles simulated spectroscopy

X-ray absorption spectra were calculated within Fermi's Golden Rule, using DFT. The initial state was derived from a ground state DFT calculation. The lowest energy final state was approximated as the self-consistent electronic response of a given molecular configuration to the presence of a core-hole on the excited carbon atom (modeled using a suitably modified pseudopotential) and the inclusion of an excited electron in the first available empty state (excited state core hole (XCH) approximation) [35]. The resulting excited state self-consistent field was used to generate subsequent higher excited states non-self-consistently. Transition matrix elements were computed using individual Kohn–Sham states (the ground state 1s atomic orbital and the spectrum of eigenvalues from the approximate final state). All DFT calculations were obtained using the PBE GGA functional [34]. Plane-wave pseudopotential calculations employed ultrasoft pseudopotentials and a kinetic energy cut-off of 25 Ry. A modified form of the Quantum-ESPRESSO package [33] was used to generate the Kohn–Sham eigenspectrum while the Shirley interpolation scheme [36] was employed to accelerate numerical convergence of computed spectra. Because there is no absolute energy reference in pseudopotential calculations, further spectral alignment was necessary for meaningful comparisons between chemically or structurally different systems. Details of the alignment scheme are described in the Results section. Isosurfaces were calculated with Quantum-ESPRESSO and rendered in VMD [37].

3. Results and discussion

3.1. Carbon dioxide vs carbonic acid

A limitation of our experiment is the uncertainty as to the species present in the acidic pH range. As the carbonate solution is mixed in the microjet with HCl to form bicarbonate and carbonic acid, it will quickly convert to dissolved carbon dioxide as shown in reactions (1)–(4). Therefore, at pH = 3, our samples in the acidic range could potentially contain carbonic acid, dissolved CO_2 , and gaseous CO_2 escaping from the microjet. The experimental on- and off-jet spectra are nearly identical after normalization, a strong indication that we are primarily observing a gaseous species. Furthermore, as shown in Figure 1, the spectra agree well with previous electron energy loss measurements for CO_2 gas [38]. However, since there are no previous NEXAFS spectra for dissolved CO_2 or carbonic acid, we must rely on theoretical spectra to establish the dominant species in this pH range.

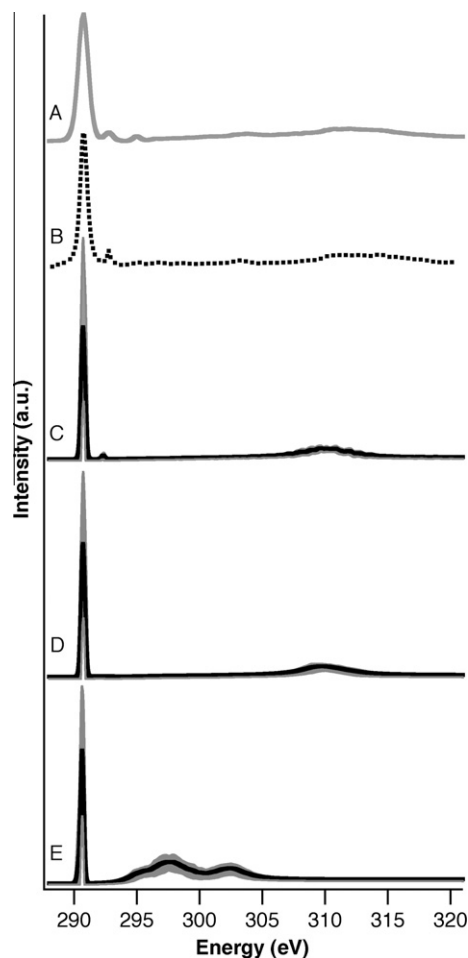


Figure 1. Experimental and calculated NEXAFS carbon K-absorption edge spectra for acidic pH range. The experimental spectrum for the acidic region (B) is compared with calculated spectra for the three possible components: CO₂ gas (C), dissolved CO₂ (D), and carbonic acid (E). The experimental ISEELS spectrum of CO₂ gas is also included (A) [38]. Each calculated spectrum represents the average of 100 individual spectra, with \pm one standard deviation shown in the shaded areas.

The calculated spectra for CO₂ gas, dissolved CO₂ and carbonic acid are compared to experiment in Figure 1. Due to the known underestimation of band gaps and band widths by DFT, the energy spacing between features will also be underestimated compared to experiment. All spectra exhibit a sharp feature at about 290.7 eV, which represents the excitation of a carbon 1s electron to the LUMO $2\pi_{u^*}$ antibonding molecular states. The shape and position of these π^* features are too similar to provide any insight into which species are actually present in the experiment. However there are distinct spectral differences in the higher energy range that provide the key to interpreting our experiments. Carbonic acid exhibits two broad σ^* resonances from 294 to 305 eV that are absent in the experiment. Both CO₂ species have broader σ^* features representing the $4\sigma_{u^*}$ resonance centered at 310 eV that match experiment, but only gaseous CO₂ exhibits the small peak observed at 292.3 eV, representing the $3s\sigma_g$ Rydberg state. Furthermore, the peak positions for the $2\pi_{u^*}$, $3s\sigma_g$, and $4\sigma_{u^*}$ peaks in the experimental spectra (Figure 1A and B) match extremely well with those observed in previous CO₂ gas electron-energy-loss spectra [39] and NEXAFS measurements [26]. Transitions to additional 3p, 4s, and 4p Rydberg states in CO₂ gas are weakly detected in the 295–297 eV range, yet these features are not resolved in our plane-wave supercell theoretical spectra due to their diffuse nature. Calculations with a larger box size will be necessary to resolve such fine structure for higher energy Rydberg states. All of the above factors clearly indicate that the dom-

inant species in our acidic pH experiment is CO₂ gas, but it is also important to understand the chemical origin of this peak.

One would assume that the disappearance of the $3s\sigma_g$ feature upon hydration is simply due to the presence of water. However, slight changes in the shape of CO₂ can also impact the position and intensity of features in the computed spectrum. There were negligible differences in the bond distances and angles between gaseous and dissolved CO₂, but to confirm the effect of hydration versus molecular shape on the spectrum, additional fictitious core-excited state calculations were performed on the CO₂ molecules with the effect of the water removed from the spectra. This constrained model maintains the structural effects of the solvent while removing the electronic confinement and hybridization effects. The constrained CO₂ gas spectrum for the $2\pi_{u^*}$ and $3s\sigma_g$ states is compared with its dissolved counterpart and the original gaseous CO₂ spectrum in Figure 2A. This indicates that the spectroscopic disappearance of the $3s\sigma_g$ feature is a direct result of hydration, while the small differences in molecular shape between CO₂ gas and its constrained form lead to a slight blue-shift in the position of the $2\pi_{u^*}$. To gain further insight into the reason why the $3s\sigma_g$ peak is only present in the gas phase, the states for corresponding snapshots in the dissolved and constrained CO₂ are imaged in Figure 2B–E. The $2\pi_{u^*}$ state is very similar in each and localized on the CO₂, therefore it should be unaffected by hydration. The $3s\sigma_g$ state for the gas is very large and diffuse, but upon hydration it hybridizes with the surrounding water to form a band of states that have mixed CO₂ $3s\sigma_g$ and water character. The formation of this energy dispersive band, together with the reduced overlap with the carbon 1s orbital due to its large spatial extent, leads to the eradication of the peak from the solvated phase spectrum.

Upon closer inspection of the final $3s\sigma_g$ Rydberg state shown for one CO₂ gas snapshot (Figure 2C), there is electron density around, but not actually on the carbon atom itself, which would imply that there should be no feature observed for this state in the carbon K-edge spectrum. The carbon $1s(\sigma_g) \rightarrow 3s\sigma_g$ transition is dipole-forbidden ($\sigma_g \rightarrow \sigma_g$) in the equilibrium molecular structure, but becomes dipole-allowed upon the inclusion of nuclear motion. We have previously encountered this issue of sampling the nuclear degrees of freedom accessible, either from zero-point motion or finite temperature, in order to accurately predict NEXAFS spectral features [40,41]. Here, we found the appearance of the $3s\sigma_g$ Rydberg state for CO₂ gas dependent on the bending vibration, which is consistent with previous predictions in the literature [42–44]. Vibronic coupling with the CO₂ bending mode along with the intensity-lending π^* resonance makes this the strongest observed Rydberg transition for CO₂. The correlation between O–C–O bond angle and the $3s\sigma_g$ peak is illustrated in Figure 3A for all 100 snapshots contributing to the average CO₂ spectrum. As expected, those closer to 180° show little or no intensity, while those with smaller angles display increasingly more intense peaks. This is due to stronger vibronic coupling as the molecule bends and the linear symmetry is broken. Furthermore, the spectra and isosurfaces for three representative snapshots are shown in Figure 3B. These illustrate the increasing *p*-character on the carbon atom as the CO₂ molecule bends away from the linear configuration. This demonstrates the importance of MD sampling in order to accurately predict the experimental spectrum. If only the relaxed linear CO₂ molecule was used for the gas phase calculation, then we would be missing this important Rydberg feature that is not only sensitive to CO₂ configuration but also to the presence of water.

3.2. Carbonate molecular structure effects

The basic and mid-range pH experiments are not nearly as complicated because the speciation clearly indicates carbonate and bicarbonate as the dominant species, respectively. However, we

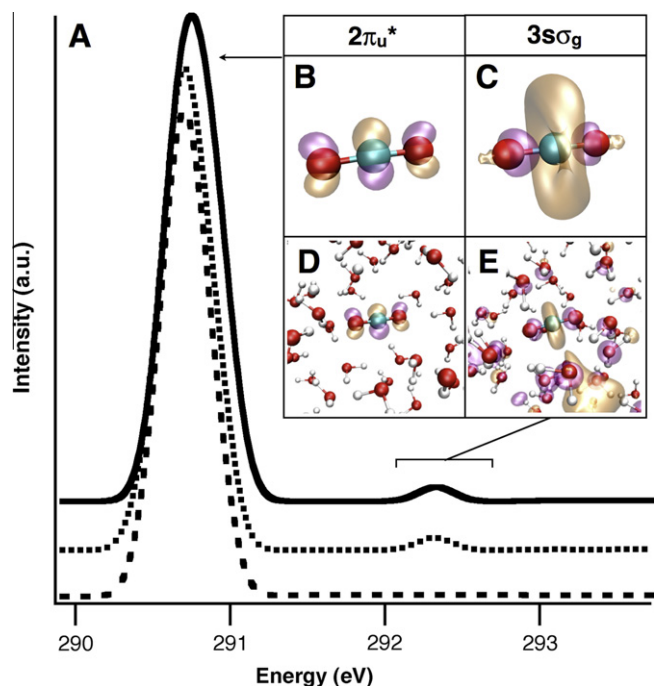


Figure 2. Spectra and isosurfaces for gaseous and dissolved CO₂. Part A shows detail of the average calculated spectra for the carbon 1s transition to the $2\pi_u^*$ and $3s\sigma_g$ states for CO₂ gas (solid line), constrained CO₂ gas (dotted line), and dissolved CO₂ (dashed line). Isosurfaces for a representative snapshot of constrained CO₂ gas are plotted in B ($2\pi_u^*$) and C ($3s\sigma_g$); and those for dissolved CO₂ in D ($2\pi_u^*$) and E ($3s\sigma_g$). Atom colors are aqua for carbon, red for oxygen, and white for hydrogen.

found it necessary to employ quantum mechanical methods to accurately model the structure and dynamics of carbonate, bicarbonate, and carbonic acid. In particular, the carbonate spectrum calculated using classical MD did not agree with experiment (Figure 4A) as a direct result of excessive flexibility in the molecular configuration. We found the LUMO π^* feature in the individual snapshots shifted to lower energy and weakened in intensity as the planar symmetry was broken via the carbon out-of-plane vibration, as measured by the C–O–O dihedral angle (Figure 5).

Further investigation into the ‘correct’ degree of planarity for carbonate revealed that other groups have also encountered too

much flexibility in this carbon out-of-plane vibrational mode (ν_2) when using classical force fields [20,45]. Previous experimental letter also indicates that the D_{3h} symmetry of the unperturbed carbonate ion is at variance with its vibrational spectrum in solution, indicating symmetry breaking of the planar structure [9,11]. Recently, Vchirawongkin et al. have calculated the degree of symmetry breaking upon hydration and confirmed that the optimized carbonate structure in water is not planar [21].

Rather than manipulate the force field parameters from the classical simulations, we instead modeled carbonate using QM/MM to better represent the appropriate flexibility of these small molecules in water. Here, the carbonate ion was treated quantum-mechanically to produce a more accurate model of the ν_2 rigidity, while the solvent was treated classically. This combination allowed for a better representation of the molecular structure while keeping the simulations tractable for the timescale needed to sample enough uncorrelated snapshots. The average absolute dihedral angle from the classical simulation was $16.5 \pm 8.5^\circ$, while QM/MM predicted a much smaller value of $2.5 \pm 2.1^\circ$. For verification of the structure, several MD trajectories were simulated using FPMD, an ab initio DFT method. In all cases, the carbonate structure equilibrated after 1 ps, with an overall average dihedral angle of $2.4 \pm 1.7^\circ$. Both QM/MM and FPMD predict that the solvated carbonate structure is still perturbed from the planar geometry, but to a much less degree than predicted classically. The NEXAFS spectrum computed from the QM/MM trajectory is in excellent agreement with the experimental spectrum (Figure 4A), indicating a much more accurate sampling of the carbonate structure with regards to the ν_2 vibrational mode. Furthermore, the bond lengths predicted by QM/MM are also in better agreement with the literature for carbonate, bicarbonate and carbonic acid. The bicarbonate spectra derived from classical MD and QM/MM are compared with experiment in Figure 4B. While we did not encounter the same problem with planarity for the bicarbonate π^* feature, the agreement with experiment was improved with QM/MM due to the more accurate prediction of bond lengths.

3.3. Spectral fingerprints of aqueous carbonate species

It is important to note that the calculated spectra are not simply aligned empirically to the corresponding experimental absorption onset energies, but, rather, relative to a simulated atomic carbon

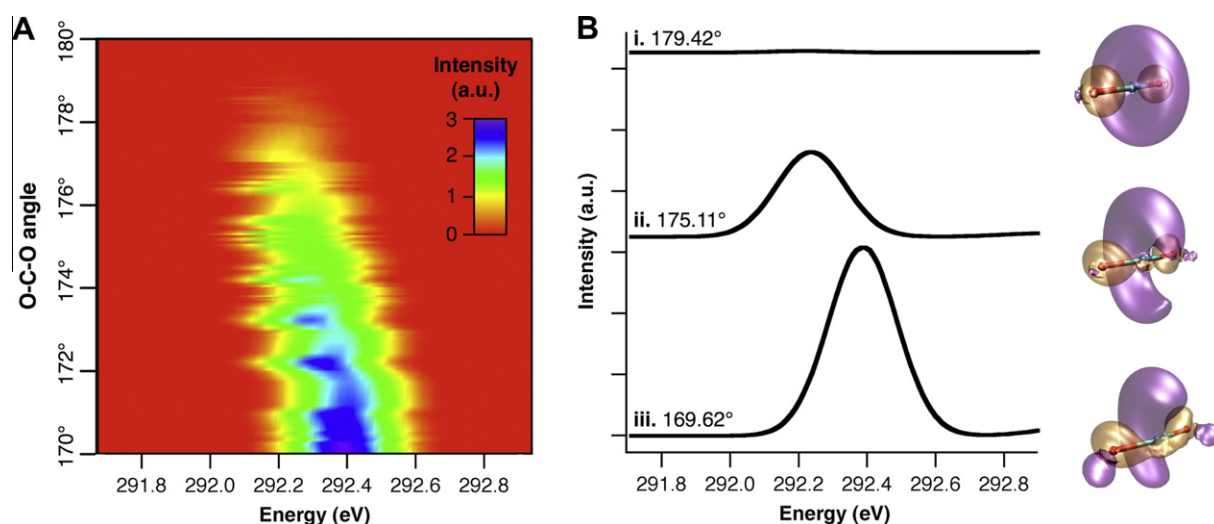


Figure 3. CO₂ $3s\sigma_g$ Rydberg vibronic state. In panel A, the $3s\sigma_g$ feature for all 100 individual CO₂ gas spectra is plotted versus energy (x-axis) and O–C–O angle (y-axis), with the peak intensity represented by rainbow color. Because this feature is vibrationally coupled to the bending mode, the intensity increases as the CO₂ angle decreases from 180°. Panel B shows three spectra representing snapshots over a range of CO₂ linearity, with their bond angles indicated and corresponding isosurfaces plotted to the side. The atom size in the isosurface plots has been minimized in order to see localization of electron density on the carbon atom.

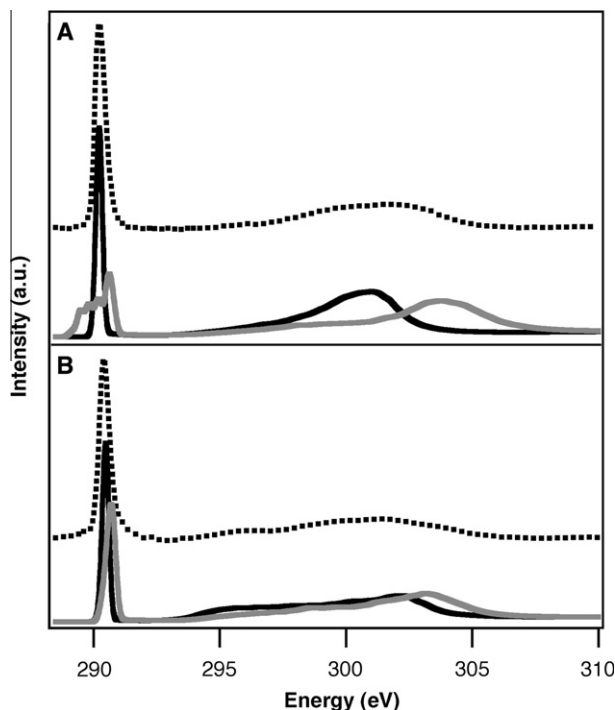


Figure 4. Carbonate and bicarbonate spectra. The experimental spectrum for the basic pH region is compared to the calculated spectra for carbonate (panel A), and the mid-range pH to bicarbonate (panel B). Experimental spectra are plotted as dotted lines, with the calculated spectra shown as solid lines (QM/MM = black and classical MD = gray). All calculated spectra represent the average of 100 individual spectra. For both carbonate and bicarbonate, the spectrum computed from QM/MM is in better agreement with experiment than the classically derived spectrum.

excitation energy. This allows us to accurately predict relative spectral energy alignment, and provides accurate absolute energies for aqueous carbonate species when aligned with an established standard measurement, such as the position of the $2\pi_{\text{u}}^*$ peak in gaseous CO_2 . Relative alignment of calculated spectra is a pervasive problem both for simulations of isolated clusters when using pseudopotentials (which neglect explicit calculation of core-electronic states) and for accurate simulations of condensed phases

using periodic boundary conditions (in which the energy reference is necessarily determined by the mathematical requirement that the potential in each repeated cell must average to zero). To overcome these limitations, we can shift the energy scale of the computed DFT eigenvalues such that relative energies between different systems are meaningful and such that we have alignment with an experimental reference.

For a given chemical system X with a molecular configuration i (possibly sampled from a molecular dynamics trajectory), we shift the energy scale used in the absorption cross section, $\sigma(E)$, as follows:

$$E \mapsto E - \epsilon_{N+1}^{\text{XCH}}(i) + \Delta E_{\text{atomic}}^{\text{C}}(i) + \Delta_{\text{expt}}, \quad (5)$$

where $\epsilon_{N+1}^{\text{XCH}}(i)$ is the $(N+1)$ th eigenvalue of the lowest energy core-excited state of configuration i , i.e., corresponding to the Kohn–Sham eigenvalue of the first available state that the excited electron could occupy above the existing N valence electrons; $\Delta E_{\text{atomic}}^{\text{C}}(i)$ is the relative excitation energy of $X(i)$ with respect to that of an isolated C atom (we only consider carbon core-level excitations in this letter), computed as:

$$\Delta E_{\text{atomic}}^{\text{C}}(i) = [E_{\text{tot}}^{\text{XCH}}(i) - E_{\text{C}}^{\text{XCH}}(i)] - [E_{\text{tot}}^{\text{GS}}(i) - E_{\text{C}}^{\text{GS}}(i)] \quad (6)$$

where these are DFT total energy differences between the total system X and the isolated atom in ground and excited states. Note that the dependence of the atomic energies on snapshot i is not necessarily unique for each snapshot, but appears only through the same choice of periodic boundary conditions (lattice vectors, cell volume, etc.). Finally the alignment with experiment is performed once and only once for a given reference calculation through the constant Δ_{expt} . In our case, only the spectrum of isolated CO_2 was aligned to the corresponding gas-phase experiment and all other simulated spectra were aligned relative to that. A similar alignment approach has been documented by Hamann and Muller for electron energy loss near-edge spectra [46]. This is a key step towards using an efficient first-principles theory to accurately predict X-ray absorption spectra of novel condensed phases.

Based on this scheme, the relative energy positioning in the calculated carbonate spectra is in excellent agreement with the experimental results, as shown in detail for the LUMO π^* feature

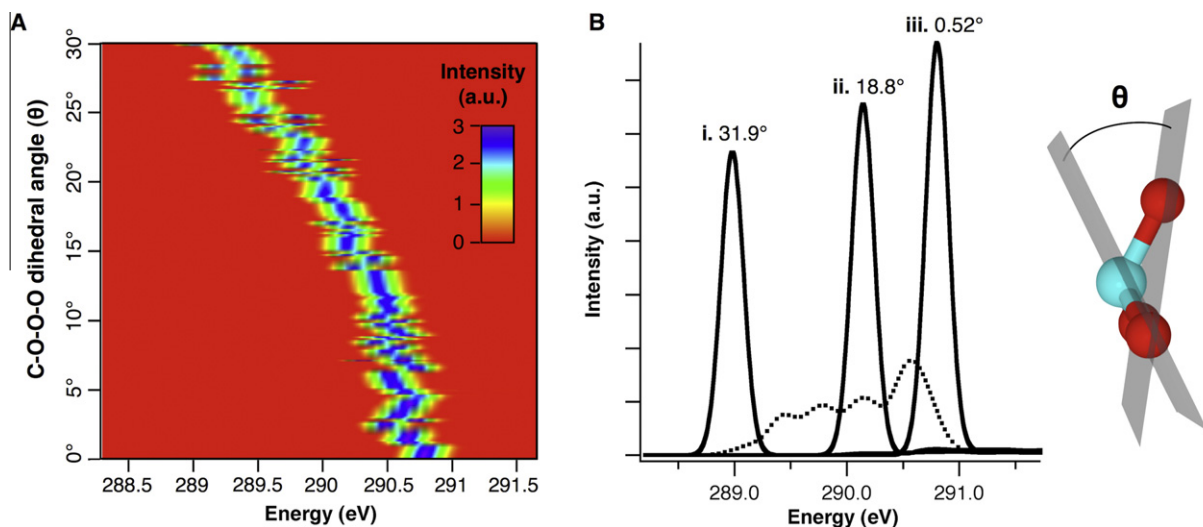


Figure 5. Carbonate dihedral angle. Panel A shows the correlation between the carbonate π^* energy (x -axis) and the dihedral angle (y -axis), with the peak intensity represented by rainbow color for all 100 individual classically-derived spectra. Panel B displays three representative spectra (solid lines) labeled with their corresponding dihedral angle, and the average of all 100 spectra (dotted line) which is also plotted in Figure 4A. The $\text{C-O}_1\text{-O}_2\text{-O}_3$ dihedral angle, θ , is also defined in panel B as the angle between the planes formed by $\text{C-O}_1\text{-O}_2$ and $\text{O}_1\text{-O}_2\text{-O}_3$. As the dihedral angle increases, the planar symmetry of the π^* final state is broken, resulting in less intense features at lower energies.

in Figure 6A. The relative ordering is reproduced correctly, and the position of carbonate matches well. The bicarbonate π^* feature is predicted to be 0.08 eV higher than experiment, but since the experimental resolution is 0.1 eV, this difference is reasonable.

Given that the X-ray excitation is localized on the carbon atom, the NEXAFS spectra are highly sensitive to its immediate surroundings, in particular to the nature of its bonds with oxygen. The C–O bond length will have significant impact on the energies of bonding and antibonding states in a molecule. A shorter bond will result in a stronger bonding interaction and consequently a higher energy antibonding state relative to a longer C–O bond. This correlation between intramolecular bond lengths and the position of K-shell resonances (especially σ^* resonances) has been documented previously for a variety of gas phase molecules [47]. A thorough analysis of the bond lengths in these molecules becomes critical to understanding the subtle differences in the spectra.

There are two types of bonds present in these molecules: C=O (or C–O⁻) and C–OH. The ordering of the calculated average C=O bond lengths follow the sequence: CO₂ (1.166 Å) < H₂CO₃ (1.224 Å) < HCO₃⁻ (1.261 Å) < CO₃²⁻ (1.285 Å), which correlates with the relative positions of the LUMO π^* carbonyl peaks (Figure 6A) and the σ^* carbonyl peaks (Figure 4B, feature 1). Additionally, C–OH bonds are present in bicarbonate (1.356 Å) and carbonic acid (1.339 Å), which introduces a third peak (Figure 6B, feature 2) in the σ^* range. The C–OH bonds are longer than the C=O bonds overall, so they appear at lower energies. All bond lengths are compiled in Table 1. For further confirmation, the states of each feature were imaged for individual snapshots to verify that they were indeed localized on the C=O or C–OH bonds, with the appropriate π^* or σ^* character (Figure 7).

3.4. Relative condensation energies

NEXAFS spectroscopy is also sensitive to the local chemical environment around the molecule, as found with the effect of hydration on the $3s\sigma_g$ Rydberg transition for CO₂. It has already been shown that CO₂, carbonic acid, bicarbonate, and carbonate all have different degrees of interaction with water [19,22,23], but in order to extract detailed chemical insight from this experiment, DFT calculations also need to be performed for the corresponding bare molecules. Instead of computing the spectra for all snapshots, only one representative snapshot was chosen for each system. The waters were stripped away and the bare molecules were allowed to relax before calculating the total energies, thereby removing both the interactions with water and any intramolecular rearrangements that occur as a result of hydration. Using the same atomic carbon alignment scheme, the relative absorption onsets (π^* peak shifts) of the bare and hydrated systems were calculated with the following ordering: carbonate (+3.16 eV) > bicarbonate (+1.22 eV) > carbonic acid (-0.067 eV) > carbon dioxide (-0.073 eV).

These peak shifts encompass the difference between the interactions of the ground and core-excited states with the solvent (analogous to solvatochromism in UV-Vis spectroscopy). They can be explained by estimating differences in condensation energy between the states. Condensation energies for the ground and excited states were calculated by subtracting all of the individual energy components from total energy of the hydrated states:

$$\Delta E_{\text{GS}}^{\text{cond}} = E_{\text{GS}}^{\text{total}} - E_{\text{GS}}^{\text{bare}} - NE_{\text{GS}}^{\text{H}_2\text{O}} - ME_{\text{GS}}^{\text{Na}^+} \quad (7)$$

$$\Delta E_{\text{XCH}}^{\text{cond}} = E_{\text{XCH}}^{\text{total}} - E_{\text{XCH}}^{\text{bare}} - NE_{\text{XCH}}^{\text{H}_2\text{O}} - ME_{\text{XCH}}^{\text{Na}^+} \quad (8)$$

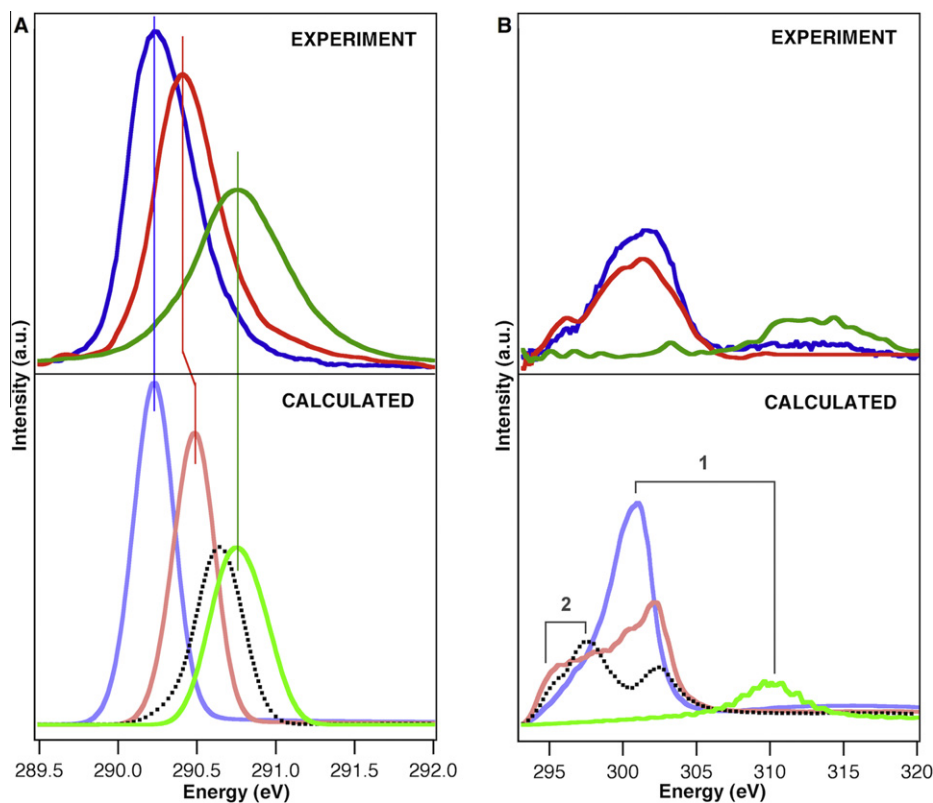


Figure 6. Experimental and calculated NEXAFS spectra for all three pH regions. The experimental spectra are presented with the corresponding calculated spectra for carbonate (blue), bicarbonate (red), and carbon dioxide gas (green). The calculated spectrum of carbonic acid (dotted black) is included for comparison. The figure is split to show the detailed alignment of the π^* features in panel A, and the σ^* resonances in panel B. Panel B is plotted on a smaller scale y-axis for better visualization of the higher-energy features. Features within the areas marked 1 and 2 in panel B represent transitions to σ^* states localized on the C=O and C–OH bonds, respectively. Calculated spectra represent the average of 100 individual snapshots.

Table 1

Average C–O bond lengths. The bond lengths (Å) calculated for this work are the averages of 100 snapshot MD trajectories with an error of one standard deviation. The literature values for CO₂ gas are experimental bond lengths, while those for the aqueous species are calculated at the B3LYP level using a polarizable continuum model for the solvent.

	This work		Literature	
	C=O (Å)	C–OH (Å)	C=O (Å)	C–OH (Å)
CO _{2(g)}	1.166 ± 0.021		1.162 ^a	
CO _{2(aq)}	1.165 ± 0.020		1.162 ^a	
	1.171 ± 0.021		1.167 ^b	
H ₂ CO _{3(aq)}	1.171 ± 0.024		1.167 ^b	
	1.224 ± 0.021	1.342 ± 0.029	1.220 ^b	1.335 ^b
HCO _{3(aq)} ⁻ (Na ⁺)	1.263 ± 0.021	1.336 ± 0.025	1.259 ^b	1.335 ^b
	1.259 ± 0.022	1.356 ± 0.027	1.255 ^b	1.397 ^b
CO _{3(aq)} ²⁻ (2Na ⁺)	1.293 ± 0.024		1.302 ^b	
	1.284 ± 0.022		1.302 ^b	
	1.279 ± 0.023		1.302 ^b	

^a Ref. [50].

^b Ref. [19].

where E_{GS}^{total} , E_{XCH}^{total} are the total energies of the hydrated system in the ground and excited states, E_{GS}^{bare} , E_{XCH}^{bare} are the total energies of the bare molecules in the ground and excited states, $E_{GS}^{H_2O}$, $E_{GS}^{Na^+}$ are the total energies of a single water molecule or sodium ion, while N and M are the number of waters and sodium ions for each system. All energies were obtained from the DFT pseudopotential calculations using the PBE GGA functional [34]. The calculated relative condensation energies (ΔE_{GS}^{cond} , ΔE_{XCH}^{cond}) for each species in eV are: CO₂ (-25.30, -25.37), H₂CO₃ (-31.85, -31.91), HCO₃⁻ (-33.96, -32.74), and CO₃²⁻ (-35.76, -32.59). It should be noted that these ‘condensation energies’, are not an absolute measure of hydration energy, but rather, a description of the relative energetic effects of the presence of water on the different carbonate species. The difference between the excited and ground state condensation energies should yield the same relative alignment provided by Eq. (6).

If both the ground and excited states were stabilized by the solvent to the same degree, then we would expect no peak shift between the bare and hydrated systems. However, we find that the ground and excited states have differing degrees of interaction with the surrounding water. The ground state of carbonate is the most stabilized upon hydration and bicarbonate to a lesser degree.

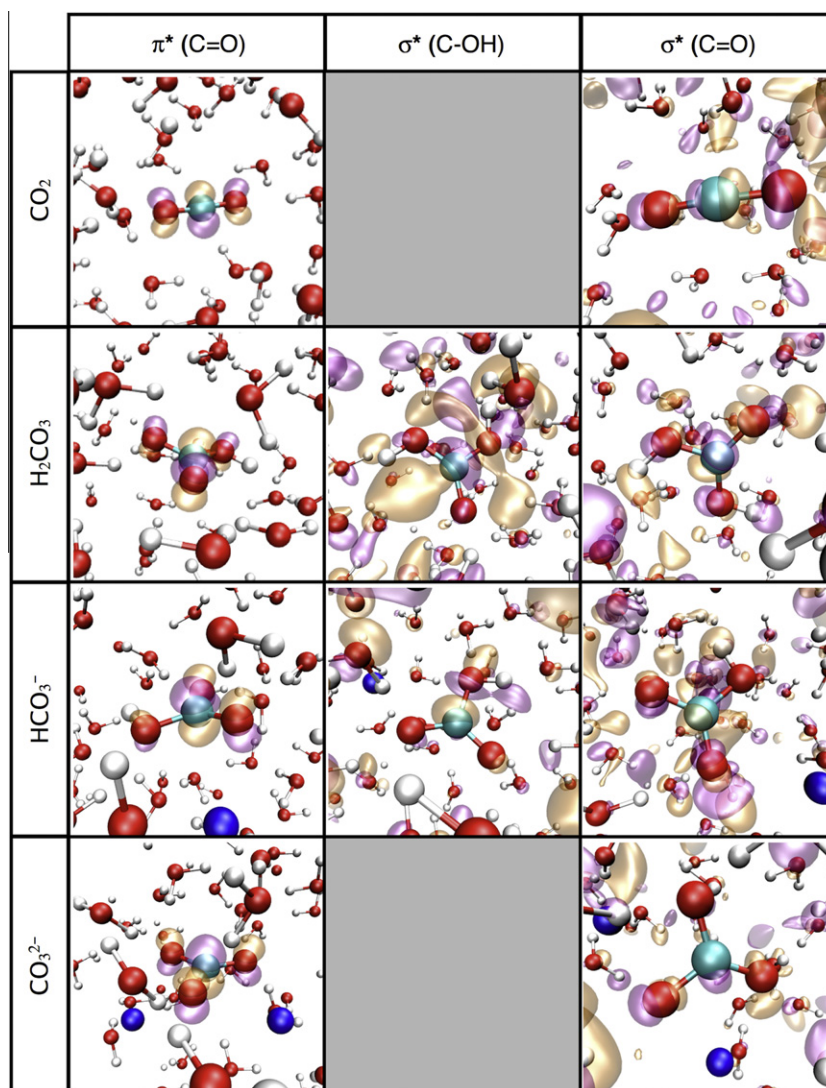


Figure 7. Isosurfaces for π^* or σ^* resonances of hydrated carbonate species. Isosurfaces illustrate the localization of π^* or σ^* resonances along C=O or C–OH bonds for each species. The π^* states correspond to the features in the calculated spectra shown in detail in Figure 6A, while the C=O and C–OH σ^* states correspond to the features in Figure 6B, designated in areas 1 and 2, respectively. Atom colors are aqua for carbon, red for oxygen, white for hydrogen, and blue for sodium. The σ^* resonances are hybridized with the surrounding water to create a large band of states, but some localization along the carbon–oxygen σ bonds can still be seen in the representative isosurfaces.

This is expected, given the double and single overall negative charge on these ions, respectively. The corresponding excited states are less stabilized, given that the solvent is in equilibrium with the solute ground state and cannot rearrange on the X-ray absorption timescale. This difference in stabilization leads to an opening of the gap between ground and excited states, resulting in a blue-shift of the absorption onset. The neutral species, carbonic acid and CO_2 , both exhibit comparatively weak interactions with water. However, their diffuse and polarizable excited states are more stabilized due to electronic screening by the solvent, leading to a small overall red-shift.

Furthermore, these energetic arguments are in accord with the number of coordinating water molecules derived from radial distribution functions of the MD trajectories. The relative ordering of $\Delta E_{\text{GS}}^{\text{cond}}$ values, $\text{CO}_2 > \text{H}_2\text{CO}_3 > \text{HCO}_3^- > \text{CO}_3^{2-}$, representative of increasing hydration strength through the series, matches with the number of coordinated waters up to 2.5 Å: CO_2 (0.56) < H_2CO_3 (3.17) < HCO_3^- (4.26) < CO_3^{2-} (5.55). This trend in hydration strength and number of coordinating waters for each species is in agreement with other theoretical studies [19,22,23] as well as with experiment for carbonate [48]. It should be noted, however, that our water coordination numbers are lower overall for bicarbonate and carbonate when compared to the literature, which is due to the inclusion of sodium counterions in our MD simulations. We found that both sodium ions were located closer to carbonate than any waters, resulting in a large decrease in the number of waters in the first solvation shell from (9.09 to 5.55). For bicarbonate, the effect was less pronounced from (5.41 to 4.26) since only one sodium ion was present and positioned near the same distance as the first hydration shell.

4. Conclusions

It was determined that the experimental NEXAFS spectrum of the acidic carbonate solution is dominated by CO_2 gas. While several previous studies have characterized the X-ray absorption spectrum of gaseous CO_2 , this work has additionally identified key spectral differences between CO_2 gas, dissolved CO_2 , and carbonic acid. The sensitivity of the $3s\sigma_g$ state to both CO_2 molecular shape (vibronic coupling with the bending mode) and to environment (gaseous versus hydrated) makes it an ideal marker to probe the behavior of CO_2 in systems relevant to carbon sequestration, such as in brine aquifers or MOFs. While the present experiment did not actually detect aqueous carbonic acid, the characteristic calculated spectrum provides an important starting point for future NEXAFS studies.

Although incorrect, the unrealistic flexibility of carbonate in our classical picture has allowed us to sample a larger range of geometries not accessible in our experiment and therefore has revealed the sensitivity of the carbon K-edge NEXAFS spectrum to the carbon out-of-plane motion in carbonate's nominally trigonal planar geometry. Future experimental research to confirm this could include monitoring the change in the π^* feature with specific excitation of the ν_2 mode, or by investigating the carbonate ion in different chemical environments or reactions where coordination contributes to symmetry breaking [49].

The calculated spectra for the species observed in these experiments (carbonate, bicarbonate, CO_2 gas) correspond well in both shape and relative alignment, which demonstrates the predictive capability of our first principles electronic structure approach for calculating NEXAFS spectra. Although not actually measured here, the relative position of carbonic acid is well-predicted, given the C–O bond length analysis of all hydrated species. Furthermore, the relative condensation energies extracted from the calculated spectra match the trends previously described in the literature.

For aqueous carbonate species, our measurements and analysis indicate that NEXAFS is sensitive to subtle differences in both chemistry and environment at the molecular scale and provide a vital benchmark for further studies of this fundamental carbon cycle.

Acknowledgements

This letter was supported by the Director, Office of Basic Energy Sciences, Office of Science, US Department of Energy under Contract No. DE-AC02-05CH11231 through Lawrence Berkeley National Laboratory's Chemical Sciences Division; experiments were performed at the Advanced Light Source, with theory, interpretation, and analysis provided through a User Project at the Molecular Foundry, and high performance computing resources provided by the National Energy Research Scientific Computing Center. Additional computing resources were provided by the Molecular Graphics and Computation Facility (College of Chemistry, University of California, Berkeley) under NSF grant CHE-0840505. A. H. England acknowledges support from the Office of Civilian Radioactive Waste Management Graduate Fellowship administered by Oak Ridge Institute for Science and Education under a contract between the US Department of Energy and the Oak Ridge Associated Universities.

References

- [1] R. Vaidhyanathan, S.S. Iremonger, G.K.H. Shimizu, P.G. Boyd, S. Alavi, T.K. Woo, *Science* 330 (2010) 650.
- [2] G.S.H. Pau, J.B. Bell, K. Pruess, A.S. Almgren, M.J. Lijewski, K.N. Zhang, *Adv. Water Res.* 33 (2010) 443.
- [3] D. Gebauer, A. Verch, H.G. Börner, H. Colfen, *Cryst. Growth Des.* 9 (2009) 2398.
- [4] P. Raiteri, J.D. Gale, *J. Am. Chem. Soc.* 132 (2010) 17623.
- [5] S.J. de Putron, D.C. McCorkle, A.L. Cohen, A.B. Dillon, *Coral Reefs* 30 (2011) 321.
- [6] T. Loerting, J. Bernard, *Chem. Phys. Chem.* 11 (2010) 2305.
- [7] D. Langmuir, *Aqueous Environmental Geochemistry*, Prentice Hall, New Jersey, 1997.
- [8] F.K. Cameron, A. Seidell, *J. Phys. Chem.* 6 (1902) 50.
- [9] A.R. Davis, B.G. Oliver, *J. Solution Chem.* 1 (1972) 329.
- [10] M. Falk, A.G. Miller, *Vib. Spectrosc.* 4 (1992) 105.
- [11] W.W. Rudolph, D. Fischer, G. Irmer, *Appl. Spectrosc.* 60 (2006) 130.
- [12] E. Garand et al., *J. Am. Chem. Soc.* 132 (2010) 849.
- [13] H. Sato, N. Matubayasi, M. Nakahara, F. Hirata, *Chem. Phys. Lett.* 323 (2000) 257.
- [14] M.T. Nguyen, M.H. Matus, V.E. Jackson, V.T. Ngan, J.R. Rustad, D.A. Dixon, *J. Phys. Chem. A* 112 (2008) 10386.
- [15] X.G. Wang, W. Conway, R. Burns, N. McCann, M. Maeder, *J. Phys. Chem. A* 114 (2010) 1734.
- [16] P. Sipos, L. Bolden, G. Hefter, P.M. May, *Aust. J. Chem.* 53 (2000) 887.
- [17] M. Perrot, F. Guillaume, W.G. Rothschild, *J. Phys. Chem.* 87 (1983) 5193.
- [18] S.G. Capewell, G. Hefter, P.M. May, *J. Solution Chem.* 27 (1998) 865.
- [19] J.R. Rustad, S.L. Nemes, V.E. Jackson, D.A. Dixon, *J. Phys. Chem. A* 112 (2008) 542.
- [20] F. Bruneval, D. Donadio, M. Parrinello, *J. Phys. Chem. B* 111 (2007) 12219.
- [21] V. Vchirawongkwin, H. Sato, S. Sakaki, *J. Phys. Chem. B* 114 (2010) 10513.
- [22] P.P. Kumar, A.G. Kalinichev, R.J. Kirkpatrick, *J. Phys. Chem. B* 113 (2009) 794.
- [23] K. Leung, I.M.B. Nielsen, I. Kurtz, *J. Phys. Chem. B* 111 (2007) 4453.
- [24] H. Falcke, S.H. Eberle, *Water Res.* 24 (1990) 685.
- [25] K. Adamczyk, M. Premont-Schwarz, D. Pines, E. Pines, E.T.J. Nibbering, *Science* 326 (2009) 1690.
- [26] T.K. Sham, B.X. Yang, J. Kirz, J.S. Tse, *Phys. Rev. A* 40 (1989) 652.
- [27] M. Bader, B. Hillert, A. Puschmann, J. Haase, A.M. Bradshaw, *Europhys. Lett.* 5 (1988) 443.
- [28] J.A. Brandes, S. Wirick, C. Jacobsen, *J. Synchrotron Radiat.* 17 (2010) 676.
- [29] K.R. Wilson et al., *Rev. Sci. Instrum.* 75 (2004) 725.
- [30] C.P. Schwartz et al., *Proc. Natl. Acad. Sci. USA* 107 (2010) 14008.
- [31] J.S. Uejio, C.P. Schwartz, A.M. Duffin, A. England, D. Prendergast, R.J. Saykally, *J. Phys. Chem. B* 114 (2010) 4702.
- [32] D.A. Case et al., AMBER 9, University of California, San Francisco, 2006.
- [33] P. Giannozzi et al., *J. Phys. Condens. Matter* 21 (2009) 295502.
- [34] J.P. Perdew, K. Burke, M. Ernzerhof, *Phys. Rev. Lett.* 77 (1996) 3865.
- [35] D. Prendergast, G. Galli, *Phys. Rev. Lett.* 96 (2006).
- [36] E.L. Shirley, *Phys. Rev. B* 54 (1996) 16464.
- [37] W. Humphrey, A. Dalke, K. Schulten, *J. Mol. Graphics* 14 (1996) 33.
- [38] A.P. Hitchcock, D.C. Mancini, *J. Electron. Spectrosc. Relat. Phenom.* 67 (1994) 1.
- [39] I.G. Eustatiu, T. Tyliczszak, A.P. Hitchcock, C.C. Turci, A.B. Rocha, C.E. Bielschowsky, *Phys. Rev. A* 6104 (2000).

- [40] J.S. Uejio, C.P. Schwartz, R.J. Saykally, D. Prendergast, *Chem. Phys. Lett.* 467 (2008) 195.
- [41] C.P. Schwartz, R.J. Saykally, D. Prendergast, *J. Chem. Phys.* 133 (2010).
- [42] J. Adachi, N. Kosugi, E. Shigemasa, A. Yagishita, *J Phys Chem-US 100* (1996) 19783.
- [43] N. Kosugi, *J Electron Spectrosc.* 79 (1996) 351.
- [44] K.C. Prince, L. Avaldi, M. Coreno, R. Camilloni, M. de Simone, *J. Phys. B-at Mol. Opt.* 32 (1999) 2551.
- [45] T.D. Archer, S.E.A. Birse, M.T. Dove, S.A.T. Redfern, J.D. Gale, R.T. Cygan, *Phys. Chem. Miner.* 30 (2003) 416.
- [46] D.R. Hamann, D.A. Muller, *Phys. Rev. Lett.* 89 (2002).
- [47] F. Sette, J. Stohr, A.P. Hitchcock, *Chem. Phys. Lett.* 110 (1984) 517.
- [48] Y. Kameda, M. Sasaki, S. Hino, Y. Amo, T. Usuki, *Physica B* 385–386 (2006) 279.
- [49] P.C. Healy, A.H. White, *Spectrochim. Acta Part A* 29 (1973) 1191.
- [50] L. Pauling, *Nature of the Chemical Bond*, Cornell University Press, New York, 1960.



Alice England was born in Salt Lake City in 1984. She obtained her B.A. in Chemistry from Vassar College in 2006. She is currently a graduate student in the group of Prof. Richard Saykally in the Chemistry Department of the University of California, Berkeley.



Andrew M. Duffin graduated with a B.Sc. in Chemistry from Brigham Young University. Afterwards he moved to the University of California, Berkeley for graduate work under the direction of Richard Saykally. While at Berkeley he studied electrokinetic effects in liquid microjets and *x*-ray spectroscopy of solvated boron compounds. Andrew received his Ph.D. from Berkeley in 2010 and is currently a postdoctoral researcher at Pacific Northwest National Laboratory.



Craig Schwartz was born in Wheaton, IL in 1983. He obtained his B.A. in Chemistry from Northwestern University in 2004. He received his Ph.D. in Chemistry from University of California, Berkeley in 2010 under the supervision of Prof. Richard Saykally. Currently he works as an Associate Predictive Modeler with AllState.



Janel Uejio was born in Concord, MA, in 1983, but was raised in Schenectady New York. She attended Carleton College where she graduated magna cum laude, in 2005 with a degree in chemistry. Her doctoral work was completed under Prof. Richard Saykally at the University of California Berkeley in 2010. She now resides in Oregon, where she works for Intel, in process development.



David Prendergast was born in Ireland in 1977. He obtained his B.Sc. in Physics and Mathematics with First Class Honors from University College Cork (UCC) in 1999 and his Ph.D. in Physics in 2002 from the group of Prof. Stephen Fahy at UCC. He has worked as a postdoctoral fellow in the groups of Giulia Galli at Lawrence Livermore National Laboratory and Steven G. Louie in the Physics Department of University of California, Berkeley. In 2007, he joined the Molecular Foundry at Lawrence Berkeley National Laboratory as a Staff Scientist where he works in the Theory of Nanostructured Materials Facility.



California, Berkeley.

Rich Saykally is a co-author of over 380 publications that have been cited over 22,000 times and the recipient of over 70 honors and awards from nine different countries. He is a member of the National Academy of Sciences and the American Academy of Arts and Sciences, is a UC-Berkeley Distinguished Teacher, and has been active at the national level in science education. Over 150 students and postdocs have trained under his direction, many of whom hold prominent positions in academic, government, and industrial institutions. Saykally currently holds The Class of 1932 Endowed Chair in the Department of Chemistry at University of